AFRL-RX-WP-JA-2022-0180

DETERMINING DEFORMATION BEHAVIOR OF AISI 9310 STEEL VARYING TEMPERATURE AND STRAIN RATE FOR AEROSPACE APPLICATIONS (POSTPRINT)

Adanma Akoma, Kevin Sala, Chase Sheeley and Lesley D. Frame

University of Connecticut

22 June 2021
Interim Report

(STINFO COPY)
AIR FORCE RESEARCH LABORATORY
MATERIALS AND MANUFACTURING DIRECTORATE
WRIGHT-PATTERSON AIR FORCE BASE, OH 45433-7750
AIR FORCE MATERIEL COMMAND
UNITED STATES AIR FORCE

REPORT DOCUMENTATION PAGE

PLEASE DO NOT RETURN YOUR FORM TO THE ABOVE ORGANIZATION.

1. REPORT DATE	2. REPORT TYPE	3. DATES COVERED	
		START DATE	END DATE
22 June 2021	Interim	1 July 2020	22 May 2021

4. TITLE AND SUBTITLE

Determining Deformation Behavior of AISI 9310 Steel Varying Temperature and Strain Rate for Aerospace Applications (Postprint)

5a. CONTRACT NUMBER	5b. GRANT NUMBER	5c. PROGRAM ELEMENT NUMBER
FA8650-20-C-5206		
5d. PROJECT NUMBER	**5e. TASK NUMBER**	**5f. WORK UNIT NUMBER**
		X1T9

6. AUTHOR(S)

Adanma Akoma, Kevin Sala, Chase Sheeley and Lesley D. Frame – University of Connecticut;

7. PERFORMING ORGANIZATION NAME(S) AND ADDRESS(ES)

University of Connecticut 352 Mansfield Road Unit 2048 Storrs CT 06269-2048;

8. PERFORMING ORGANIZATION REPORT NUMBER

9. SPONSORING/MONITORING AGENCY NAME(S) AND ADDRESS(ES)	10. SPONSOR/MONITOR'S ACRONYM(S)	11. SPONSOR/MONITOR'S REPORT NUMBER(S)
Air Force Research Laboratory Materials and Manufacturing Directorate Wright-Patterson Air Force Base, OH 45433-7750 Air Force Materiel Command United States Air Force	AFRL/RXMS	AFRL-RX-WP-JA-2022-0180

12. DISTRIBUTION/AVAILABILITY STATEMENT

DISTRIBUTION STATEMENT A. Approved for public release. Distribution is unlimited;

13. SUPPLEMENTARY NOTES

PA Case Number: AFRL-2021-1937; Clearance Date: 22 June 2021. This document contains color. Journal article published in Heat Treating Conference Proceedings, online 14 September 2021. © 2021 ASM International. The U.S. Government is joint author of the work and has the right to use, modify, reproduce, release, perform, display, or disclose the work. The final publication is available at https://doi.org/10.31399/asm.cp.ht2021p0196

14. ABSTRACT

Determination of flow stress behavior of materials is a critical aspect of understanding and predicting behavior of materials during manufacturing and use. However, accurately capturing the flow stress behavior of a material at different strain rates and temperatures can be challenging. Non-uniform deformation and thermal gradients within the test sample make it difficult to match test results directly to constitutive equations that describe the material behavior. In this study, we have tested AISI 9310 steel using a Gleeble 3500 physical simulator and Digital Image Correlation system to capture transient mechanical properties at elevated temperatures (300°C – 600°C) while controlling strain rate (0.01 s-1 to 0.1 s-1). The data presented here illustrate the benefit of capturing non-uniform plastic strain of the test specimens along the sample length, and we characterize the differences between different test modes and the impact of the resulting data that describe the flow stress behavior.

15. SUBJECT TERMS

9310 Steel, Deformation behavior, Flow stress, Strain rate, Temperature;

16. SECURITY CLASSIFICATION OF:			17. LIMITATION OF ABSTRACT	18. NUMBER OF PAGES
a. REPORT	b. ABSTRACT	C. THIS PAGE		
Unclassified	Unclassified	Unclassified	SAR	9

19a. NAME OF RESPONSIBLE PERSON	19b. PHONE NUMBER *(Include area code)*
Elizabeth Loiacono	(937) 904-4398

PREVIOUS EDITION IS OBSOLETE.

STANDARD FORM 298 (REV. 5/2020)
Prescribed by ANSI Std. Z39.18

Heat Treat 2021: Proceedings of the 31st ASM Heat Treating Society Conference
September 14–16, 2021
America's Center, St. Louis, Missouri, USA
DOI: 10.31399/asm.cp.ht2021p0196

Determining Deformation Behavior of AISI 9310 Steel Varying Temperature and Strain Rate for Aerospace Applications

Adanma Akoma, Kevin Sala, Chase Sheeley, Lesley D. Frame

Materials Science and Engineering
University of Connecticut, Storrs, CT, United States of America
adanma.akoma@uconn.edu, lesley.frame@uconn.edu

Abstract

Determination of flow stress behavior of materials is a critical aspect of understanding and predicting behavior of materials during manufacturing and use. However, accurately capturing the flow stress behavior of a material at different strain rates and temperatures can be challenging. Non-uniform deformation and thermal gradients within the test sample make it difficult to match test results directly to constitutive equations that describe the material behavior. In this study, we have tested AISI 9310 steel using a Gleeble 3500 physical simulator and Digital Image Correlation system to capture transient mechanical properties at elevated temperatures (300°C – 600°C) while controlling strain rate (0.01 s^{-1} to 0.1 s^{-1}). The data presented here illustrate the benefit of capturing non-uniform plastic strain of the test specimens along the sample length, and we characterize the differences between different test modes and the impact of the resulting data that describe the flow stress behavior.

Introduction

Deformation behavior for a given ductile metal is dependent on temperature, strain rate, and prior processing. Understanding the flow stress and deformation behavior is useful for manufacturing process sequences and specific thermal and mechanical parameters. However, measurement of the flow stress at a range of temperatures and strain rates can be challenging. In particular, it can be difficult to control all test parameters precisely as well as to capture the material behavior during non-uniform deformation and when thermal gradients are present.

The importance of accurately capturing such in-process materials properties is well established. Prediction of materials behaviors using finite element (FE) methods during manufacturing has become a primary focus of many aerospace industry companies. However, accuracy of FE models is limited by the accuracy and richness of the materials data supplied as input. Of particular interest is an ability to accurately model thermal and mechanical processes of alloys at high temperatures and a wide range of strain rates. Assessing the material behavior at various conditions provides a foundation for predicting material behavior at any processing condition.

One method for determining deformation behavior of ductile alloys is through mechanical testing at different temperatures and strain rates in order to identify parameters for accepted constitutive relationships. One such relationship is the Johnson-Cook (JC) material model. This model is often described mathematically as:

$$\sigma = \underbrace{(A + B\varepsilon^n)}_{\text{Part I}}\underbrace{(1 + C\ln\dot{\varepsilon}^*)}_{\text{Part II}}\underbrace{(1 - T^{*m})}_{\text{Part III}}$$

Where, σ is the flow stress, A is the yield stress of the material at a reference condition, B is the strain hardening coefficient, n is the strain hardening exponent, C is the strain rate sensitivity coefficient, and m is the thermal softening exponent. In this model, strain hardening (Part I), strain rate sensitivity (Part II), and thermal softening (Part III) are each considered [1]. The general trend for most ductile alloys is that strain hardening is positive (at higher strains, strength increases), as strain rate increases, strength also increases, and as temperature increases, strength decreases. The JC model has been heavily applied across a wide range of engineering alloys under many loading conditions, and there is considerable focus on steel alloys in the literature [2]-[7]. However, the model does not consider all softening mechanisms that can occur during straining. In particular, the model does not consider dynamic recrystallization and dynamic grain growth. Other models consider these mechanisms that may contribute to softening or strengthening, including the Baman-Chisea-Johnson model and the EMMI models [8],[9]. The literature and landscape quickly thicken with complementary and competing models of the flow stress behavior of materials.

Regardless of the constitutive relationship or model under consideration, the collection of materials data is fundamental to our understanding of the behavior. In this study we have captured flow stress materials property data for AISI 9310 steel under a range of temperature and strain rate conditions. We have considered a range of experimental conditions that can influence the results and our interpretation of the materials behavior. This may serve as a guide for future studies that attempt to capture such properties experimentally.

Methods

The primary method for characterizing the flow stress behavior of our AISI 9310 steel samples was with a Gleeble 3500 physical simulator. This instrument allows control of specimen temperature, stroke position, and strain rate while monitoring load. In addition, we used a Correlated Solutions Digital Image

Correlation system to monitor strain along the entire specimen length during testing.

Gleeble Sample Preparation

AISI 9310 steel rods normalized to AMS 6265 were machined to round tensile samples with dimensions as indicated in Figure 1. The reduced diameter region of the samples was lightly sanded with fine 600 grit SiC paper and wiped down with ethanol to remove any oxides and oils from prior handling in preparation for thermocouple attachment. Two 30 AWG type K thermocouples (TC) were spot welded to the specimens using a DSI 35200A thermocouple welder kit at 34V. As indicated in Figure 1, TC1 was placed at the approximate center of the sample to drive the temperature control, and TC2 was placed at the "off-center" position to capture the thermal gradient. The position of TC2 varied among the tests, and the purpose of the second TC was to determine the thermal gradient along the length of the specimen. Measurements of TC placement were taken using a Holex digital caliper.

(a)

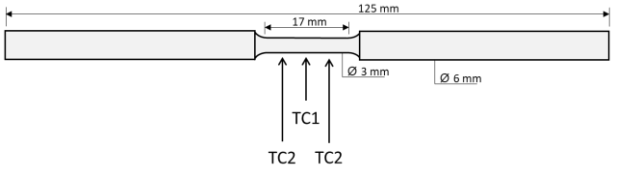

(b)

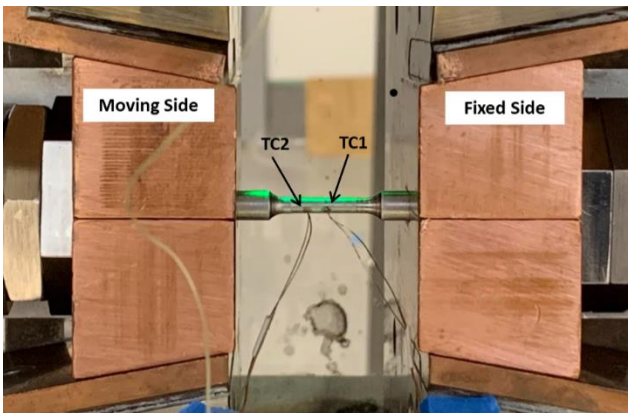

Figure 1. Samples were prepared for Gleeble testing by attaching two Type K thermocouples as indicated here. (a) sample geometry is shown with reduced diameter section along a 17 mm gage length. TC1 was attached at the mid-point, and TC2 was attached off-center. Thermocouple #1 (TC1) was always selected to set the target temperature of the sample, while thermocouple #2 (TC2) was used to monitor the temperature distribution during testing. (b) The sample in place in the Gleeble fixture is shown.

The reduced diameter section was of sufficient length (17 mm) to maximize the test region in the Gleeble fixture while also creating a region of uniform temperature for testing. The specimens for Gleeble testing are heated through direct resistance heating (Joule heating effect) and the copper sample blocks are chilled to ensure proper electrical contact and enable sample cooling. There is necessarily a thermal gradient along the length of the sample.

Gleeble Test Conditions

Samples were pulled in uniaxial tension under vacuum (0.51 Torr). While this study has included test temperatures of 300°C to 600°C and strain rates of 0.01 s^{-1} to 1 s^{-1}, we report here only the 300°C results due to space constraints. The heating rate was set to 10°C/sec, and temperature was held for up to 60 seconds for stabilization prior to straining. Tests were conducted in both *stroke control* and *strain rate control* modes.

In *stroke control mode*, the Gleeble is instructed to move the sample grips, which are mounted on a piston, in a single direction at a specified rate. In *strain rate control mode*, the desired strain rate is specified, and the machine is in a dynamic testing mode where it is constantly adjusting the stroke based on feedback from an external micrometer device, such as a C-Gauge or optical micrometer. For this study, strain feedback was provided through Keyence optical micrometer incorporated into the Gleeble system. Additionally, Digital Image Correlation (DIC) was used to monitor strain during testing.

In the present study, six tests were conducted at 300°C with a target strain rate of 0.05 s^{-1}. The test conditions are reported in Table 1. Test 6032 produced thermal gradient data, but the strain data rendered the flow stress results unusable.

Table 1. Test conditions for the results reported here.

Sample Number	Control Mode	DIC
6028	Strain	No
6031	Stroke	No
6032	Stroke	No
6033	Stroke	Yes
6034	Stroke	Yes
6035	Strain	Yes

Digital Image Correlation (DIC)

DIC is a non-contact technique used to capture strain measurements during deformation. During mechanical testing, two cameras are positioned at a fixed angle to view the sample. Images are collected to capture strain in the specimen, and subsequent analysis of the images allows quantification of strain as a function of time and position along the specimen. We used a Correlated Solutions system with VIC Snap and VIC 3D software.

Setting up a test for DIC capture requires that the specimen contain a randomized speckle on the viewable surface. Samples were painted with high temperature white base coat and high temperature black speckle coat as illustrated in Figure 2. Thermocouple wires were attached prior to painting, and considerable care was taken to ensure that the paint only covered the reduced diameter portion of the samples by masking off the ends with tape. The speckle coating must be uniform and include a fine enough random speckles to ensure that the strain magnitude of interest is measurable by the system.

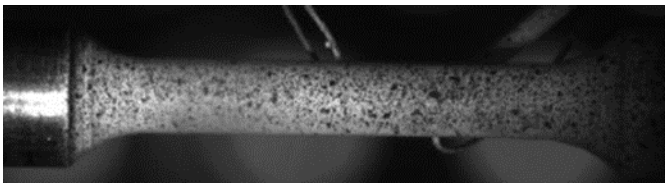

Figure 2. Specimen with speckle coating applied (specimen diameter is 3 mm).

With the specimen in place in the Gleeble fixture, the DIC cameras were positioned to view the sample from the back side of the Gleeble 3500. Cameras were angled at 20-25º apart. The lighting, focus, aperture, and exposure were each adjusted to ensure adequate view of sample. After the cameras were setup, the DIC was calibrated to the specific configuration using a 3mm grid. After setup and calibration, the DIC was started seconds before the Gleeble tests began to ensure the entire test was captured.

The DIC images were evaluated using the VIC 3D software. Correlation between images at several locations along the sample were manually confirmed, and rigid body motion was subtracted prior to calculating the true transverse strain. Strain is reported here at specific locations along the specimen. In particular, we report the strain at the thermocouple 1 (TC1) and thermocouple 2 (TC2) positions. The DIC data was synched to the Gleeble output data based on the image time stamps and the onset of strain in the specimen.

Results

One of the key challenges to capturing flow stress data for materials at elevated temperatures is the need to consider the inevitable thermal gradients that are present in the specimen. Figure 3 shows the thermal distribution along the reduced diameter section of the test specimens for all of the tests reported here. The TC1 thermocouples are indicated, and it is important to note that these are the reference thermocouples for each test. This means that the Gleeble is controlling temperature based off of these thermocouple values, so each TC1 result should be at or very near the set point of 300ºC. The TC2 thermocouples are distributed along the specimens, and while the distribution in Figure 3 illustrates excellent clustering of the temperature at the middle of the reduced diameter section, any given test only included two thermocouples. These TC1/TC2 pairings are indicated in Figure 3 by the color coding. Taken together, these data suggest that there is a rapid decline in temperature away from the TC1 location. Within 4mm, the temperature can drop by almost 30 degrees. Additionally, these data represent the temperature distribution prior to testing the sample. During testing, some samples experienced rather high adiabatic heating, resulting in greater thermal gradients and temperature fluctuations. These variations are apparent in the charts that follow.

Because of the generally accepted behavior of ductile alloys described above, one might expect that the region with the highest temperature will also be the region of highest deformation and fracture. However, this was not necessarily the case. In Figure 4, three of the test specimens are shown. From these images it is clear that necking and fracture did not correlate well with the highest temperature location. The non-uniform temperature certainly influenced the deformation behavior of the samples, but it was not the only factor at play.

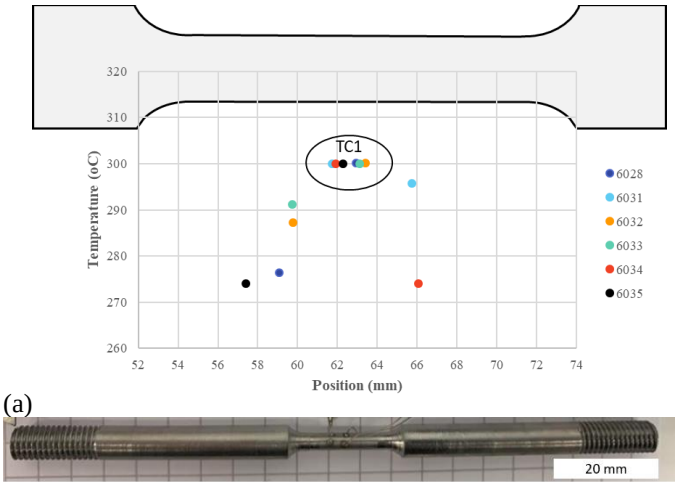

Figure 3. (a) Temperature distribution along the reduced diameter section. The schematic of the specimen is aligned with the position scale in the chart to illustrate the relative position of the thermocouples. TC1 was located between 61.74 mm and 63.42 mm along the length of the 125 mm samples. TC2 was positioned on the left or right of TC1 for the tests. (b) One of the specimens with thermocouple wires welded in place is shown.

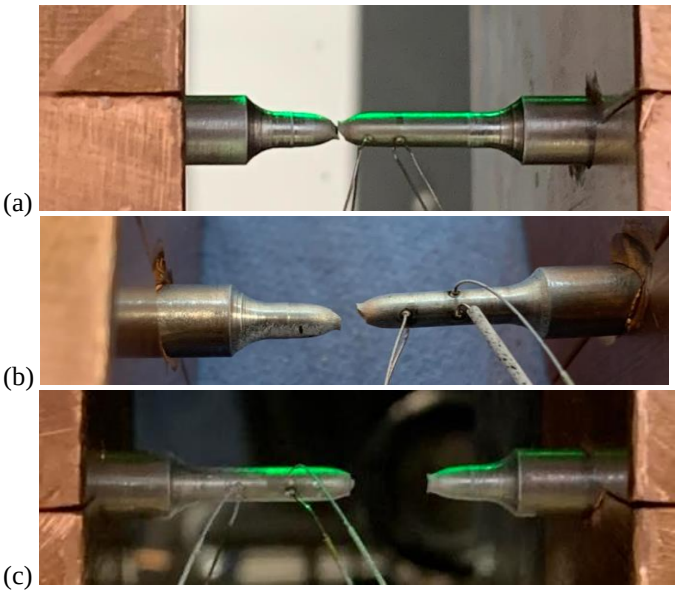

Figure 4. (a) 6032 fractured specimen with TC2 positioned on the left. (b) 6034 fractured specimen with TC2 positioned on the right. (c) 6035 fractured specimen with TC2 positioned on the left.

Typical Gleeble output data will allow determination of strain, stress and temperature throughout the test period. In Figures 5 and 6, these data are reported. Figure 5 shows the strain rate controlled sample 6028 results and Figure 6 shows the stroke controlled sample 6031 results. In the strain rate control mode,

it is clear that there are actually four different strain rate regions, and each will impact the flow stress behavior of the material differently. The initial rapid strain rate results in rapid stress increase and as the strain rate decreased, the stress dropped in both tests. This behavior qualitatively matches the expectation that rapid strain rates result in higher strengths.

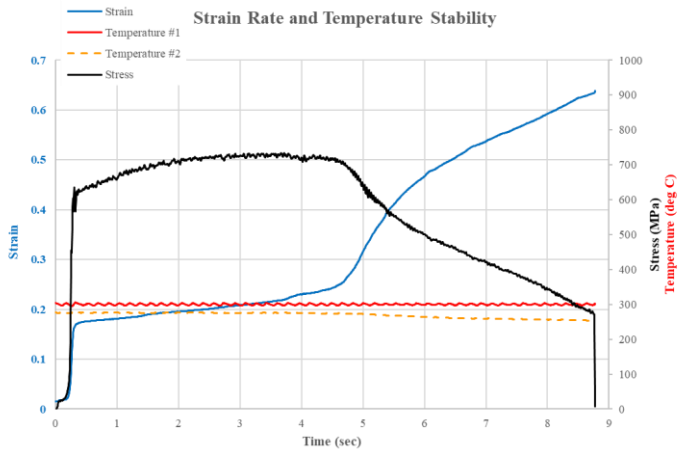

Figure 5. Sample 6028, strain rate control mode. Strain measured by optical micrometer for the Gleeble system. Note that the temperature at TC1 and TC2 locations were stable, but the strain rate varied.

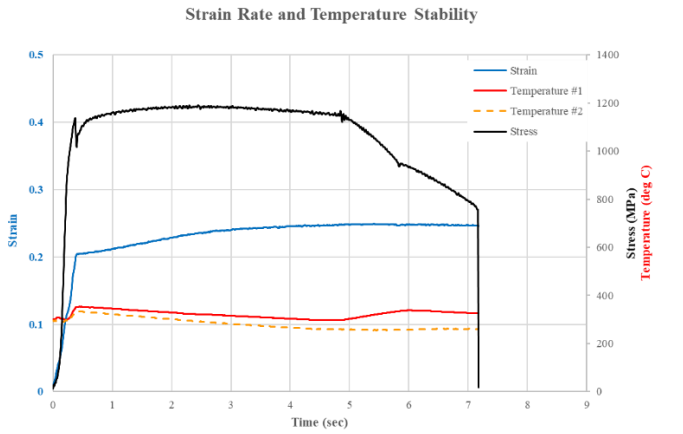

Figure 6. Sample 6031, stroke control mode. Strain measured by optical micrometer for the Gleeble system. Note that the temperature at TC1 and TC2 locations fluctuated slightly during the test, but the strain rate was very stable.

Plotting the flow stress from these tests can be misleading when taken out of the context of variable strain rate and thermal gradients in the sample. Figures 7 and 8 show the stress and inverse strain rates for these tests, and it is clear that the flow stress behavior is markedly different depending on the strain rate throughout the test. Further, the prior strain rate appears to influence the subsequent flow behaviors during the test. Both tests show that the transition from the initially high strain rate to the much lower (and more stable) strain rate results in a dip in stress. This is most likely due to recovery in the specimen due to the elevated temperature. The target strain rate for both tests was 0.05 s^{-1}, but the actual strain rate varied from as high as 2.26 s^{-1} during initial loading to as low as 0.06 s^{-1} during necking just before fracture.

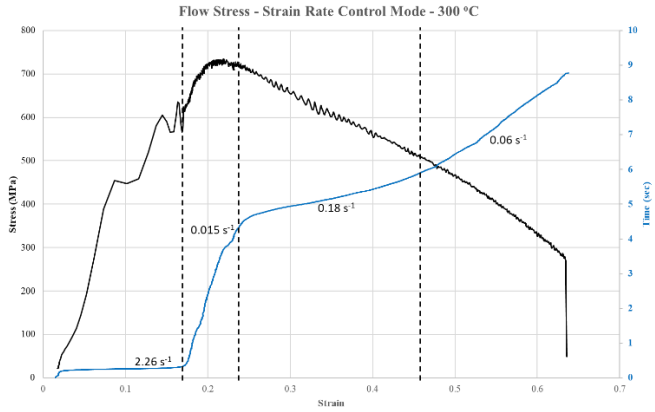

Figure 7. Sample 6028 showing flow stress behavior and inverse strain rate. Strain rates for the four identified regions are indicated.

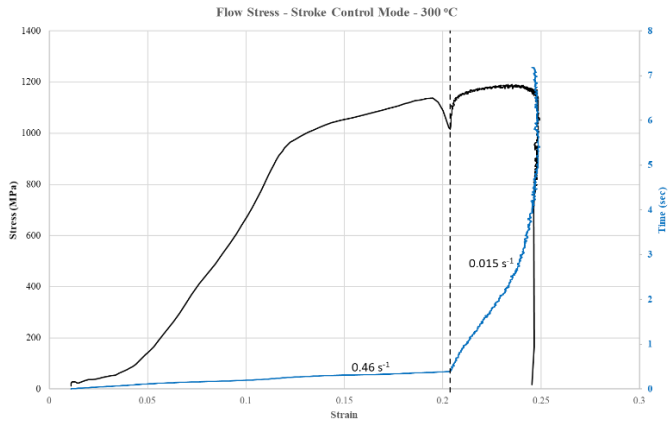

Figure 8. Sample 6031 showing flow stress behavior and inverse strain rate. Strain rates for the two regions are indicated.

Tests 6033, 6034, and 6035 were conducted with the DIC system. This method of examination proved highly valuable when determining variation in strain along the length of the specimens during testing. Figure 9 illustrates the relative transverse strain distribution along the reduced diameter length for specimen 6035. Note that there is much greater strain to the right of TC1 even though this image reflects sample deformation prior to necking. The location of fracture for this specimen aligns with the region in red for Figure 9 (see Fig. 4c for comparison).

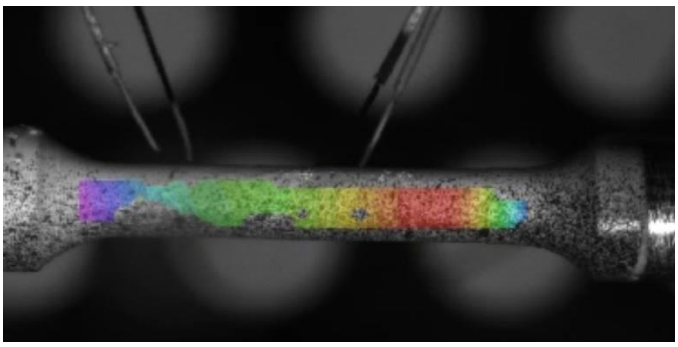

Figure 9. Sample 6035 showing relative strain along the sample length. Red indicates highest region of strain.

Figures 10, 11 and 12 illustrate the output data verses time including both the Gleeble data and the strain at TC1 and TC2 positions as determined using the DIC system. Notice that while the general trends for strain and stress values determined from the DIC results match the Gleeble data well, the specific values are quite different. In particular, Figure 10 showing sample 6033 shows that the strain at TC2 position is much higher than TC1 position even though the temperature value is very close. In Figures 11 and 12, the strain at the TC1 location is greater, and Figures 13 and 14 show corresponding DIC images at points during uniform elongation and at necking. In both of these tests, necking occurred adjacent to the TC1 location, and it is clear that the higher strain noted at the TC1 location relates to its proximity to the eventual point of necking (perhaps more than the temperature difference between TC1 and TC2).

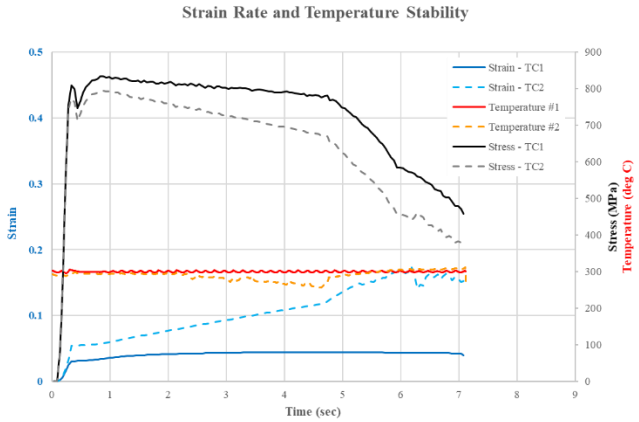

Figure 10. Sample 6033, stroke control mode. Strain measured by DIC system along the entire sample length. Note that the temperature at TC2 fluctuated slightly during the test, but the strain rate at TC1 location was very stable.

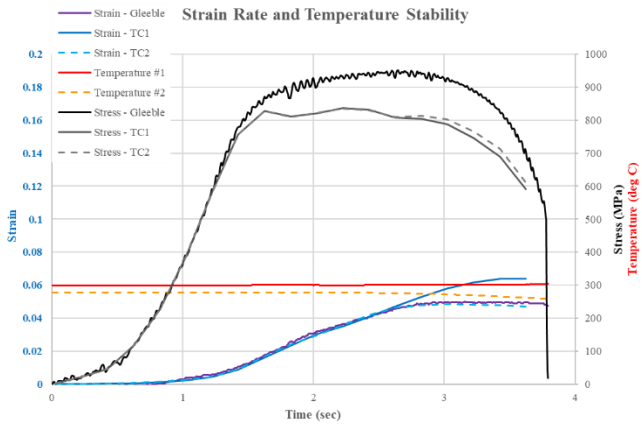

Figure 11. Sample 6034, strain control mode. Strain measured by DIC system along the entire sample length and the Gleeble optical micrometer between TC1 and TC2. Temperature was stable during the test. The strain at all measured positions was consistent.

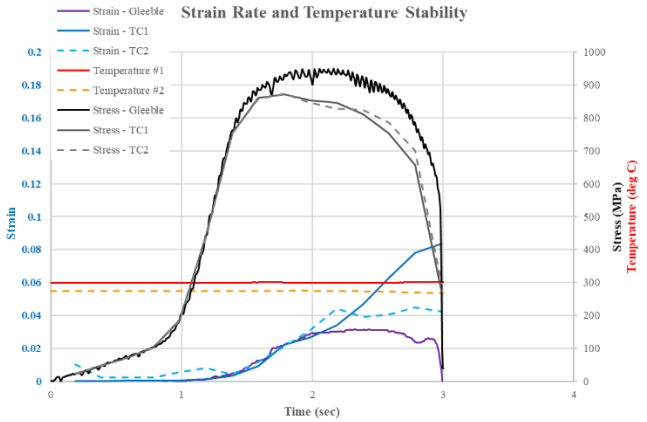

Figure 12. Sample 6035, stroke control mode. Strain measured by DIC system along the entire sample length and the Gleeble optical micrometer between TC1 and TC2. Temperature was stable during the test. The strain at TC1 position was much higher than the strain at TC2 and at the point where the Gleeble optical micrometer was set.

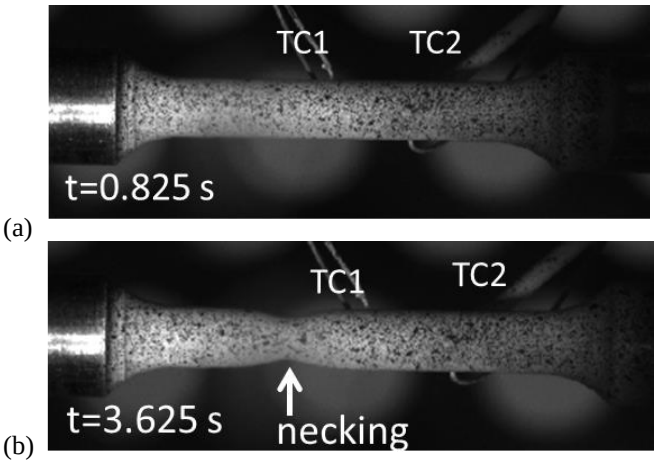

Figure 13. DIC images for sample 6034 during uniform elongation (a) and after onset of necking (b).

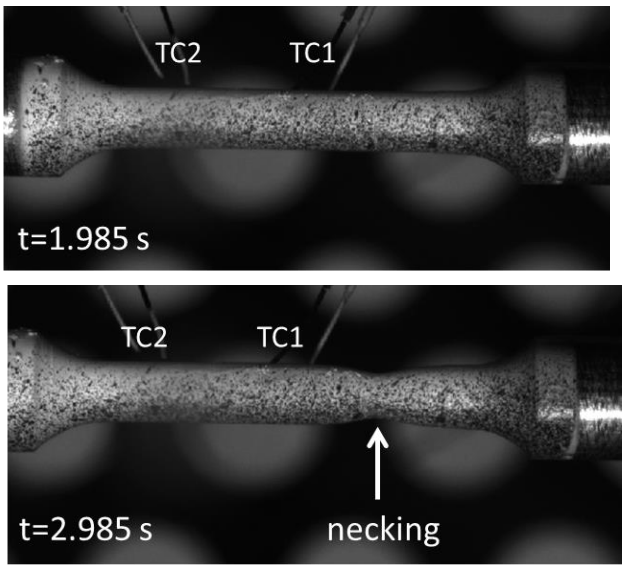

Figure 14. DIC images for sample 6035 during uniform elongation (a) and after onset of necking (b).

The corresponding flow stress curves for samples 6033, 6034, and 6035 are shown in Figures 15 – 17. Here we see that there are similar strain rate transitions in sample 6033, but samples 6034 and 6035 had more uniform strain rate. An additional challenge that is apparent from these charts is the noise in the optical micrometer measurement and the lack of data points from the DIC system. In two of the tests (6034 and 6035) the frame rate was insufficient and resulted in gaps in the strain observation during testing.

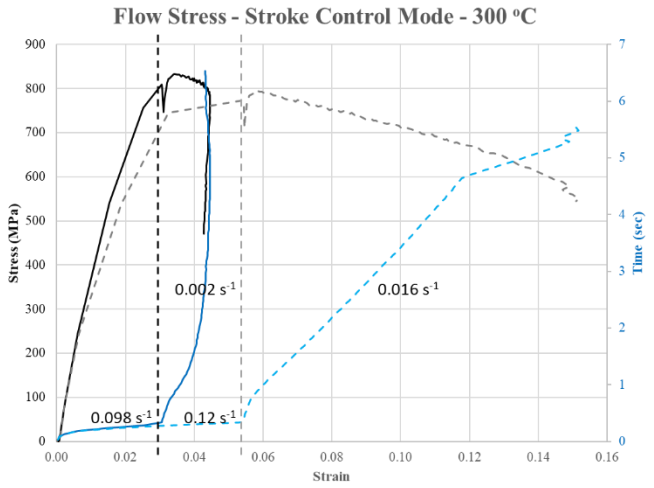

Figure 15. Sample 6033, showing flow stress behavior and inverse strain rate at TC1 and TC2 positions. Notice that strain rates for the two regions at each of the TC locations are indicated.

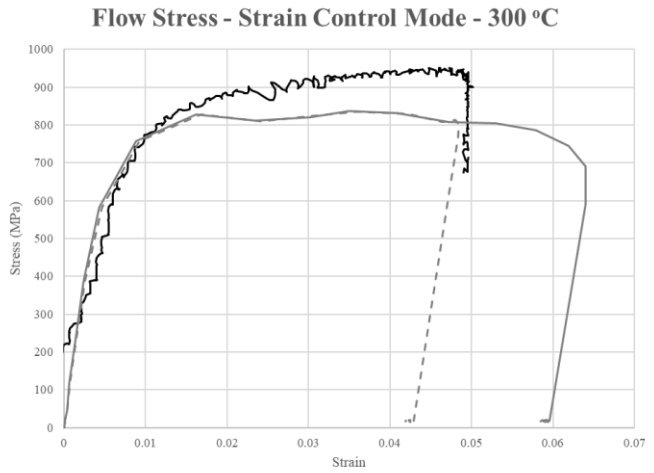

Figure 16. Sample 6034, showing flow stress behavior from the Gleeble optical micrometer and at TC1 and TC2 positions measured by DIC.

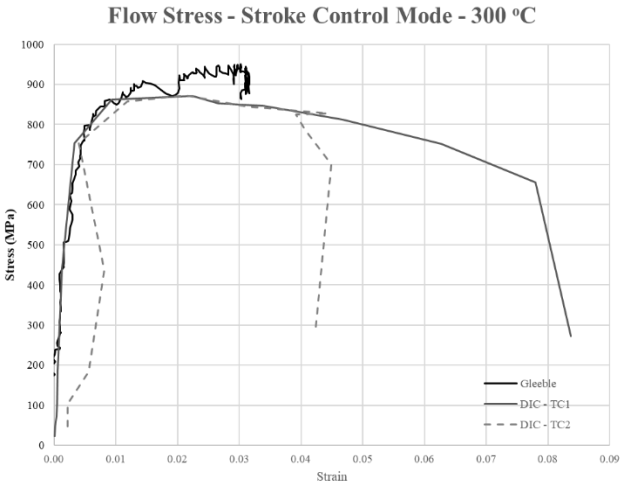

Figure 17. Sample 6035, showing flow stress behavior from the Gleeble optical micrometer and at TC1 and TC2 positions measured by DIC.

With the flow stress curves presented here, it is possible to determine strain hardening behavior for the AISI 9310 material. Table 2 summarizes the strain hardening coefficient (JC parameter, B) and the strain hardening exponent (JC parameter, n). As indicated in this table, the values cannot be taken at face value. Instead, this illustrates the need for further validation of the flow stress results. The very high strain hardening coefficient and exponent from sample 6028 is likely due to the rapid initial strain rate (2.26 s^{-1}) prior to the stable strain rate of 0.015 s^{-1}. Sample 6033 and the DIC determined strains for samples 6034 and 6035 indicated that softening mechanisms are at play in these specimens.

Test	Measurement Location	Strain Rate	B (MPa)	n
6028	Gleeble	0.015	2198	0.7
6031	Gleeble	0.015	1543	0.183
6033	DIC - 1	0.002	440	-1.92
6033	DIC - 2	0.015	439	-0.212
6034	Gleeble	0.027	1323	0.108
6034	DIC (1 & 2)	0.03	781	-0.014
6035	Gleeble	0.027	1219	0.076
6035	DIC (1 & 2)	0.05	664	-0.063

Conclusion

As gathered from the results previously stated, there is more to be understood of the relation of properties and processing parameters of AISI 9310 steel. When temperature, strain and strain rate all vary, the influence on deformation behavior is not direct. When solely observing the relation of temperature and deformation, areas of the sample where the temperature increased were not necessarily where necking occurred, as indicated in Figure 4a-b. This observation is contrary to expected behavior. Additionally, temperature is influenced by

the deformation of the material. As indicated by Figure 6 and Figure 10, variation in temperature is evident during testing.

When examining the flow stress behavior, it was determined that the material strength was influenced by the strain rate. In regions of higher strain rate, an increase of strength was evident as indicated in Figure 6 and Figure 7. This observation is in good agreement with the expected outcome that higher strain rate results in greater strength.

However, it is important to take into consideration the nonuniform distribution of temperature and strain along the length of the sample, as this influences the interpretation of the resulting data and our prediction of the material's behavior. As indicated in Figures 13a and 14a, uniform elongation is present in the beginning of the tests, but necking and failure occur in somewhat unpredictable locations that do not necessarily correspond to placement of thermocouples or extensometers.

Furthermore, when comparing results from the Gleeble and DIC, it is important to note the discrepancies in the stress-strain curves. As indicated in Figures 15 and 16, variation is exhibited in the flow stress curves due to the noise in the optical micrometer measurements associated with the Gleeble. On the other hand, the strain measurements gathered from the DIC system are insufficient due to the lack of data points. Due to these inconsistencies, the values cannot simply be entered into the JC or other model as-is.

In conclusion, comprehensive evaluation of non-uniform strain and temperature gradients along the specimen during flow stress testing can provide valuable insight to the real materials behavior. Such detailed observation of materials behavior is useful when establishing predictions and determining parameters for constitutive relationships describing mechanical behaviors.

Acknowledgements

Deepest appreciation goes to the Air Force Research Laboratory for funding this work, the AFRL Program Manager Elizabeth Loiacono, AFRL project leader, Dr. Pamir Alpay, and the AFRL Project Manager at UConn, Alexandra Merkouriou. We also thank Matt Beebe for machining assistance and Dr. Rainer Hebert for assistance with the Gleeble 3500. We also gratefully acknowledge the Air Force Research Laboratory, Materials and Manufacturing Directorate (AFRL/RXMS) for support via Contract No. FA8650-20-C-5206.

References

[1] G.R. Johnson, W.H. Cook, "A constitutive model and data for metals subjected to large strains, high strain rates and high temperatures," *Proceedings of Seventh International Symposium on Ballistics*, The Hague, The Netherlands, April 1983 pp. 541–547.

[2] Y.C. Lin, *et al.*, "Prediction of 42CrMo steel flow stress at high temperature and strain rate," *Mechanics Research Communications*, Vol. 35, No. 3 (2008),p 142-150. doi: 10.1016/j.mechrescom.2007.10.002

[3] J.Q. Tan, *et al.*, "A modified Johnson–Cook model for tensile flow behaviors of 7050-T7451 aluminum alloy at high strain rates." *Materials Science and Engineering: A*, Vol. 631 (2015), p 214-219. doi: 10.1016/j.msea.2015.02.010

[4] M. Murugesan and D. Won Jung, "Johnson Cook material and failure model parameters estimation of AISI-1045 medium carbon steel for metal forming applications," *Materials*, Vol. 12, No. 4 (2019), p 609. doi:10.3390/ma12040609

[5] D. Snyder, *et al.*, "Deformation characteristics and recrystallization response of a 9310 steel alloy," *Metallurgical and Materials Transactions A*, Vol. 44, No. 1 (2013), p 479-493. doi: 10.1007/s11661-012-1381-4

[6] U.J. Souza and M.F. Amateau, "Deformation of metastable austenite and resulting properties during the ausform-finishing of 1 pct carburized AlSl 9310 steel gears." *Metallurgical and Materials Transactions A*, Vol. 1, No. 30 (1999), p 183-193. doi: 10.1007/s11661-999-0206-6

[7] H.Y. Li, *et al.*, "A modified Johnson Cook model for elevated temperature flow behavior of T24 steel," *Materials Science and Engineering A*, Vol. 577 (2013), p 138–146. doi:10.1016/j.msea.2013.04.041

[8] E.B. Marin, *et al.*, "On the Formulation, Parameter Identification and Numerical Integration of the EMMI Model: Plasticity and Isotropic Damage," In Report No. SAND2006-0200 (January 2006).

[9] A.A. Brown and D.J. Bammann, "Validation of a model for static and dynamic recrystallization in metals," *International Journal of Plasticity*, Vol. 32–33 (2012), p 17–35. doi:10.1016/j.ijplas.2011.12.006